RESEARCH ARTICLE

Rapid transport of insulin to the brain following intranasal administration in rats

Lir-Wan Fan, Kathleen Carter, Abhay Bhatt, Yi Pang*
Department of Pediatrics, University of Mississippi Medical Center, Jackson, MS, USA

Funding: *This study was supported by Michael. J. Fox Foundation (to YP).*

Abstract

We previously reported that intranasal insulin protects substantia nigra dopaminergic neurons against 6-hydroxydopamine neurotoxicity in rats. This study aimed to assess insulin pharmacokinetics in the rat brain following intranasal application. Recombinant human insulin (rh-Ins) or phosphate buffer solution was administered to both nostrils of rats. Animals were sacrificed at 15 minutes, 1, 2, and 6 hours to determine insulin levels in different brain regions by an ultrasensitive, human-specific enzyme-linked immunosorbent assay kit. For fluorescence tracing study, rats were administered with intranasal florescence-tagged insulin (Alex546-Ins), and brains were fixed at 10 and 30 minutes to prepare sagittal sections. rh-Ins was detected in all brain regions examined except the cerebral cortex. The highest levels were detected in the brainstem, followed by the cerebellum, substantia nigra/ventral tegmental area, olfactory bulb, striatum, hippocampus, and thalamus/hypothalamus. Insulin levels reached a peak at 15 minutes and then declined gradually overtime, but remained significantly higher than baseline levels at 6 hours in most regions. Consistently, widespread Alex546-Ins-binding cells were detected in the brain at 10 and 30 minutes, with the olfactory bulb and brainstem showing the highest while the cerebral cortex showing lowest fluorescence signals. Double-immunostaining showed that Alex546-Ins-bindings were primarily co-localized with neuronal nuclei-positive neurons. In the subtantia nigra, phospho-Akt was found to be activated in a subset of Alex546-Ins and tyrosine hydroxylase double-labeled cells, suggesting activation of the Akt/PI3K pathway in these dopaminergic neurons. Data from this study suggest that intranasal insulin could effectively reach deep brain structures including the nigrostriatal pathways, where it binds to dopaminergic neurons and activates intracellular cell survival signaling. This study was approved by the Institutional Animal Care Committee at the University of Mississippi Medical Center (protocol 1333A) on June 29, 2015.

***Correspondence to:**
Yi Pang, MD, PhD,
ypang@umc.edu.

orcid:
0000-0003-0453-6921
(Yi Pang)

doi: *10.4103/1673-5374.250624*

Received: *October 24, 2018*
Accepted: *December 14, 2018*

Key Words: *dopaminergic neurons; striatum; substantia nigra; brainstem; olfactory bulb; glia; trigeminal nerve; pharmacokinetics; axonal transport; pAkt*

Chinese Library Classification No. *R453; R361; R741*

Introduction

As a protective mechanism for maintaining brain homeostasis, the blood-brain barrier (BBB) restricts the access of large molecules into the brain parenchyma from systemic circulation. While this feature is imperative for brain health at the physiological condition, it becomes a major hurdle in developing biological-based drugs to treat central nervous system (CNS) disorders. For example, animal studies have shown that neurotrophic factor therapy is a promising treatment for Parkinson's disease (PD), yet those proteins must be administered by non-systemic means such as local injection in order to retain sufficient levels in the target areas (Domanskyi et al., 2015; Sulivan and O'Keeffe, 2016; Sampaio et al., 2017; Barua and Gill, 2018). This drawback greatly holds back the translational potentials of neurotrophic factor therapy. A major strategy in the current CNS drug delivery research is to boost drug transport at the interface of BBB using multiple approaches, such as increasing the permeability of BBB by focused ultrasound, facilitating receptor-mediated transport and endocytosis, and modifying drug configuration by approaches such as nanomaterials, liposome, and biodegradable polymers (Shah et al., 2013; Patel et al., 2017; Zhou et al., 2018). An alternative strategy is to bypass the BBB *via* the nose-to-brain pathway, which is known for decades and is currently used clinically for delivery of certain non-peptide drugs. As for chronic neurological conditions, intranasal insulin therapy for dementia and/or Alzheimer's disease (AD) is one of the most intensively studied areas (Avgerinos et al., 2018).

Insulin receptors (IR) and accessory proteins are widely distributed in the brain (Pomytkin et al., 2018); however, the major function of insulin is not related to regulating glucose transport in neurons and glial cells. Despite its well-known central effects on regulating energy metabolism and synaptic plasticity, insulin could also act like neurotrophic factors to activate the PI3K pathway in neurons (Ramalingam and Kim, 2016). Therefore, intranasal insulin could hold therapeutic potential for not only the AD but also other neurodegenerative disorders. For example, intranasal insulin was shown to be neuroprotective in animal models of various CNS disorders, including human immunodeficiency virus infection (Mamik et al., 2016), traumatic brain injury (Brabazon et al., 2017), and stroke (Lioutas et al., 2015). In a previous study, we reported that intranasal insulin significantly increased the survival of substantia nigra (SN) dopaminergic (DA) neurons and ameliorated motor behavioral deficits in 6-hydroxydopamine-lesioned rats (Pang et al., 2016). Therefore, the present study is to further extend our previous work by assessing insulin bioavailability and potential bio-

logical response in the nigrostriatal pathway following intranasal administration of recombinant human insulin (rh-Ins).

Material and Methods

Animals and treatment

A total of 35 adult male Sprague-Dawley rats (250 g, from Envigo, Denver, CO, USA) were used. Rats were allowed to acclimate to the Laboratory Animal Facility for 1 week before experiments. On the day of treatment, rats were anesthetized by inhalation of isoflurane (Henry Schein Animal Health, Dublin, OH, USA) and laid on a supine position, and a 10 μL (20 μg) bolus of rh-Ins (Cell Science, Newburyport, MA, USA) dissolved in phosphate buffer solution (PBS) was applied to each of the nasal cavity using a 10 μL pipette. Rats were kept on the supine position under anesthesia for an additional 5 minutes, and then returned to their cages. At 15 minutes, 1, 2, and 6 hours following intranasal treatment, rats were sacrificed to prepare fresh brain tissue. Brains were quickly micro-dissected into the following regions: the olfactory bulbs (OB), striatum, thalamus plus hypothalamus, hippocampus, subtantia nigra (SN) plus ventral tegmental area (VTA), cerebellum, brainstem, and cerebral cortex. Tissues were snap-frozen in dry ice and stored at –80°C.

For fluorescence tracing study, Alexa Fluor 546-labeled insulin (Alex546-Ins; Nanocs Inc., Farmingdale, NY, USA; 10 μg in 10 μL PBS for each nostril) was applied to rats in the same way as described above. At 10 and 30 minutes, rats were deeply anesthetized and rapidly perfused intracardially with ice-cold saline followed by 4% paraformaldehyde. Brains were post-fixed in 4% paraformaldehyde for 2 hours and then cut into free-floating sagittal sections (45 μm thickness) using a microtome (Leica Biosystems, Buffalo Grove, IL, USA). This study was conducted in strict accordance with the National Institutes of Health Guide for the Care and Use of Laboratory Animals and approved by the Institutional Animal Care Committee at the University of Mississippi Medical Center (protocol 1333A) on June 29, 2015.

Enzyme-linked immunosorbent assay (ELISA)

Brain tissues were weighted before extracting total protein. Tissues were homogenized by sonication in 2× volume of Tissue Lysis Buffer supplemented with protease inhibitor cocktails (ThermoFisher Scientific, Waltham, MA, USA). Tissue lysis was centrifuged at 12,000 × *g* for 10 minutes, and the supernatant was transferred to a new Eppendorf tube. Total protein concentration was determined by BCA method (Smith et al., 1985). For ELISA, 100 μL of tissue supernatants were used in 96-well plate format. Two positive control samples were included in each ELISA: a serum sample from diabetes patients (supplied in the ultrasensitive human insulin ELISA kits from Alpco, Salem, NH, USA) and a diluted sample of rh-Ins (100 pg/mL diluted in lysis buffer). Results were presented as pg/mg wet tissue.

Immunohistochemistry

To directly visualize Alex546-Ins distribution, sections were stained with 4′,6-diamidino-2-phenylindole (DAPI, 0.2 μM in PBS) for 10 minutes, briefly washed with PBS, and mounted on slides. For co-labeling Alex546-Ins with neuronal markers or pAkt, double or triple immunofluorescence staining was performed. Sections were blocked with 10% normal goat serum and 0.5% triton in PBS for 30 minutes at room temperature and incubated with primary antibodies: neuronal nuclei (NeuN) at 1:500 (Sigma, St. Louis, MO, USA), tyrosine hydroxylase (TH) at 1:800 (Sigma), insulin at 1:400 (Santa Cruz Biotechnology, Hercules, CA, USA), and pAkt at 1:300 (Cell Signaling Technology, Danvers, MA, USA)) overnight at 4°C. The next day, sections were washed with PBS and then incubated with secondary antibodies conjugated with biotin, Alexa Fluor 488 (1:400), or Alexa Fluor 350 (1:400) (ThermoFisher Scientific, Grand Island, NY, USA) at room temperature for 1 hour. Sections were washed in PBS, mounted on slides, and air dried. DAPI (100 nM) was included in the mounting medium if necessary. Sections were viewed under a fluorescence microscope (Nikon NIE, Nikon Instruments Inc., Melville, NY, USA) and images were acquired by Nikon Nis Element software (Nikon Instruments Inc.).

Statistical analysis

Due to a highly skewed distribution, data were first log transformed and then analyzed by one-way analysis of variance (ANOVA; for a normal distribution) or one-way ANOVA on rank (for non-normal distribution), followed by Bonferroni or Dunn's *post hoc* analysis. All comparisons were made between time-points within insulin treatment (15 minutes to 6 hours) and the control (0 minute) for a particular brain region, and $P < 0.05$ is considered statistically significant.

Results

Spatiotemporal profiles of brain insulin distribution

The specificity of the ELISA kit for rh-Ins was first validated based on positive controls of human insulin and rat samples from the control group. The calculated concentration of two positive controls in each ELISA consistently reached within 5% range of predicted values. The concentration of rh-Ins from PBS-treated control rats were all below detectable limit, therefore they were assigned a value of 0. As shown in **Table 1**, significant amounts of rh-Ins were detected in all brain regions except the cerebral cortex in rh-Ins-treated rats. Rh-Ins reached the peak value at 15 minutes and declined substantially overtime, but remained significantly higher than baseline levels in most regions at 6 hours. Neither the dorsal or ventral division of the cortex showed a significant increase over baseline at any time points.

Fluorescence tracing revealed specific binding of insulin to neurons in various brain regions

Since ELISA data suggest that insulin levels peaked in less than 1 hour, we next examined brain insulin distribution by fluorescence microscopy at 10 and 30 minutes. Rat brains were rapidly perfused and fixed following intranasal administration of Alex546-tagged rh-Ins, and serial sagittal sections were prepared for either directly examining red fluorescence bindings by fluorescence microscopy, or com-

Table 1 Recombinant human insulin concentration (pg/mg tissue) in different brain regions over a 6-hour period

	0 minute	15 minutes	60 minutes	120 minutes	360 minutes
OB	0	179.5±62.0*	133.7±54.4*	39.4±6.5*	31.9±7.6*
Striatum	0	198.1±101.3*	74.8±28.1*	16.3±5.1*	7.7±2.0*
SN/VTA	0	217.6±73.8*	92.7±15.3*	40.4±12.2*	47.6±7.0*
Hippocampus	0	140.9±82.6*	47.2±5.9*	8.3±4.9	11.8±4.5
Thalamus/hypothalamus	0	92.7±29.0*	16.8±6.7	8.7±8.7	32.2±13.4*
Brainstem	0	257.9±175.6*	185.1±98.5*	110.2±29.3*	45.6±7.2*
Cerebellum	0	260.0±166.3*	153.6±63.4*	86.7±81.0*	20.4±4.2*
Dorsal cortex	0	41.8±25.6	20.3±7.9	0	0
Ventral cortex	0	0	18.35±8.0	5.4±1.4	0

Data represent mean ± SEM from five rats in each group. $*P < 0.05$, *vs.* 0 minute (one-way analysis of variance followed by Bonferroni *post hoc* analysis). OB: Olfactory bulb; SN: subtantia nigra; VTA: ventral tegmental area.

bined with immunohistochemistry for further identification. The results showed that bright red fluorescence was widely distributed in the brain. Consistent with ELISA results, we found that the OB and brainstem are two regions showing the most intense fluoresce signals, but other regions including the cerebellum, SN/VTA, hippocampus, and striatum, also showed substantial fluorescence bindings, while the cerebral cortex especially the outer layers (I–IV) showed very little signals (**Figure 1**), although scattered fluorescence-tagged cells were noted in deep layers (V–VI). When comparing fluorescence intensity at 10 and 30 minutes, there were no significant differences noted in OB, brainstem, cerebellum, but it apparently increased in deeper structures such as the thalamus and SN-VTA regions (**Figure 1G & H**).

Based on the morphology of DAPI-stained nuclei, the majority of red fluorescence labeled cells appeared to be neurons but not glial cells, suggested by their relatively larger size and more circular and lightly staining pattern as compared to their smaller, irregular, and intensely stained nuclei of glial counterparts (Purves et al., 2001). To confirm this, double-immunostaining with NeuN was performed, and the results showed that, indeed, most of the Alex546-Ins-bindings were on the membrane of $NeuN^+$ neurons, which is clearly demonstrated in the SN regions (**Figure 2A–C**). Moreover, the distribution of Alex546-Ins-binding cells was heterogeneous. For example, the majority of Alex546-Ins bindings were localized on hippocampal CA pyramidal neurons but not surrounding glial cells (**Figure 2D–F**), while in the cortex, scattered fluorescence-labeled cells were only found in the deeper layer (**Figure 2G–I**). We also determined the specificity of red fluorescence bindings by immunostaining with anti-human specific insulin antibody. We found that the red fluorescence bindings were co-localized with anti-human insulin immunoreactivity (**Figure 2J–L**), suggesting that the red fluorescence was from specific binding of Alex546-Ins but not unlabeled fluorescence.

Activation of pAkt in insulin-binding neurons including DA neurons in the SN

Our next step was to assess insulin bioavailability and biological signaling in the SN by examining the distribution of

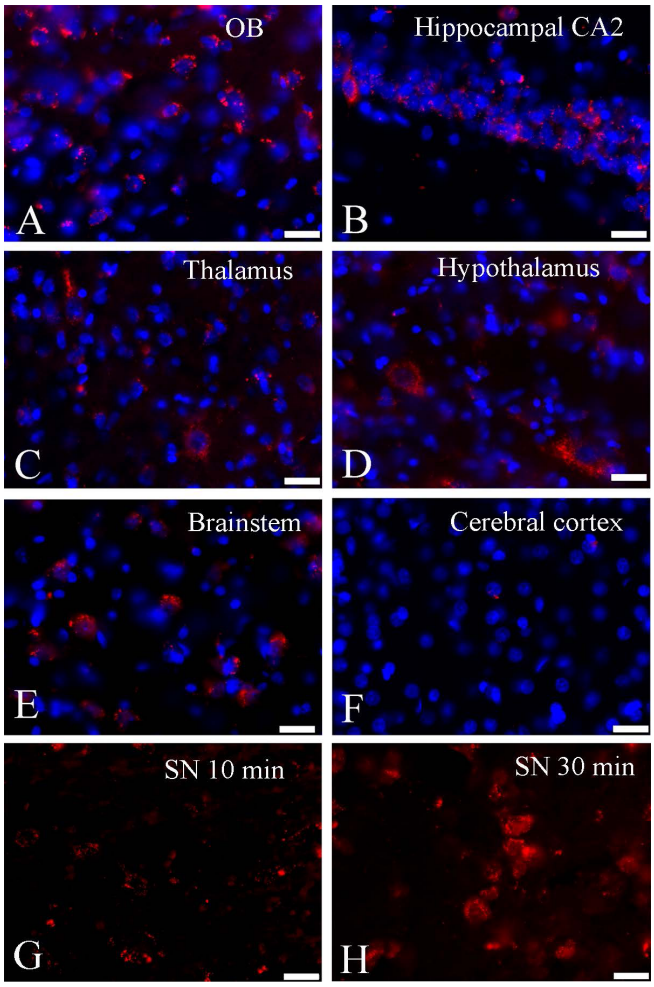

Figure 1 Distribution of Alex546-insulin binding cells in the rat brain following intranasal application.
Alex546-Ins binding cells were found widespread in the rat brain. Representative images showing Alex546-binding cells (red) in the OB (A), hippocampus CA2 (B), thalamus (C), hypothalamus (D), brainstem (E), and cerebral cortex (F) at 30 minutes. Although fluorescence intensity was similar in the OB and brainstem, it was significantly increased in the SN from 15 minutes (G) to 30 minutes (H). Nuclei were counted-stained with DAPI (blue) in A–F. Scale bars: 50 μm. OB: Olfactory bulb; SN: subtantia nigra; DAPI: 4′,6-diamidino-2-phenylindole.

Alex546-Ins binding cells and downstream signaling of IR in the SN area by immunofluorescence. First, we determined whether Alex546-Ins bind to DA neurons, using double-labeling of NeuN and TH combined with Alex546-Ins. As shown in **Figure 3**, some of the TH^+ neurons co-localized with Alex546-Ins, suggesting that once reaching SN area, insulin could bind to DA neurons and possibly induce biological responses. Indeed, double-immunolabeling showed that pAkt was activated in those DA neurons, but not in the SN of control rat brains (**Figure 4**).

Discussion

Here we showed that intranasal insulin could rapidly gain access to not only the olfactory area and brainstem, two regions known to retain a significant amount of insulin or other peptides following intranasal application, but also deep structures including the striatum, thalamus, and SN. Moreover, we provide evidence that insulin could activate Akt signaling in DA neurons of the SN, suggesting that insulin could act like a neurotrophic factor to protect DA neurons against degeneration.

Insulin is produced by pancreatic beta cells to regulate blood glucose in the periphery, while in the CNS, it is a multifaceted peptide regulating a number of brain functions including satiety, neurodevelopment, synaptic plasticity, and energy metabolism (Zemva and Schubert, 2014). In homeostasis, the levels of brain insulin are likely reflective of mixed central and peripheral origins. Glial cells synthesize insulin de nova, while insulin could also be transported from the blood to the brain by active transporters at the interface of BBB (Ghasemi et al., 2013). However, the latter mechanism is limited in its capacity so that systemic administration of insulin unlikely achieve therapeutic concentrations in the brain, not to mention potential serious complications of this approach. For these concerns, the intranasal route has been

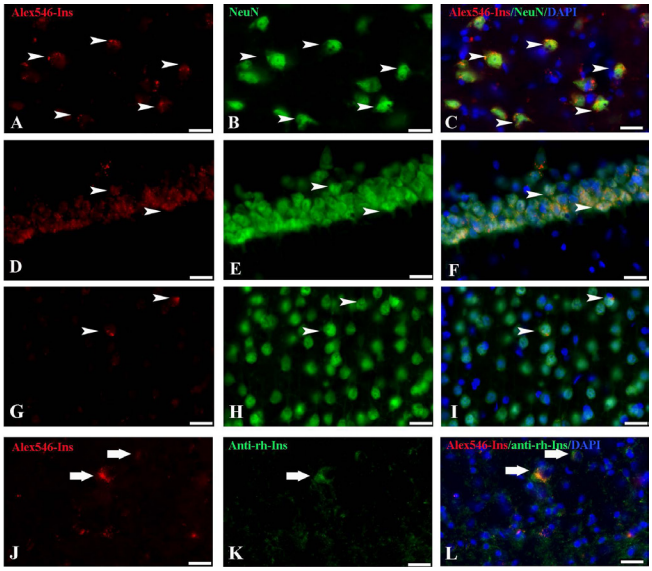

Figure 2 Alex546-insulin primarily binds to neurons.
Alex546-Ins bindings, which appeared to be localized on cell membranes, co-localized with $NeuN^+$ cells across different brain regions (indicated by arrowheads). Representative images show double-labeling in the SN (A–C), hippocampus CA1 (D–F), and dorsal layer IV of cerebral cortex (G–I). The red fluorescence labeling also showed positive immunoreactivity with anti-human specific insulin antibody (arrows in J–L). Scale bars: 50 μm. NeuN: Neuronal nuclei; SN: Subtantia nigra; DAPI: 4′,6-diamidino-2-phenylindole.

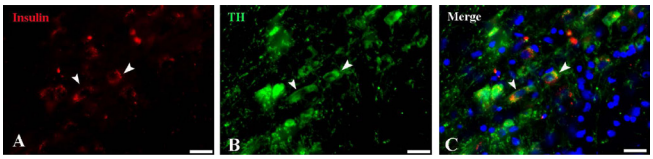

Figure 3 Identification of Alex546-insulin binding cells in the SN.
Immunostaining showed co-localization of Alex546-insulin with some of the TH^+ neurons in the SN (arrowheads, A–C). Nuclei were counter-stained with DAPI. Scale bars: 50 μm. SN: Subtantia nigra; TH: tyrosine hydroxylase; DAPI: 4′,6-diamidino-2-phenylindole.

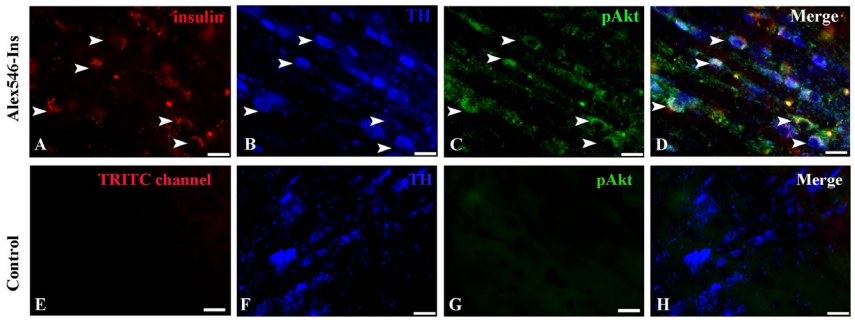

Figure 4 Activation of pAkt in dopaminergic neurons of the SN at 30 minutes following intranasal insulin administration.
Double-immunostaining showed that pAkt was activated in Alex546-insulin binding TH^+ neurons in the SN of insulin-treated rats (arrowheads in A–D), which was non-detectable in the controls (E–H). Scale bars: 50 μm. pAkt: Phosphorylated Akt; SN: subtantia nigra; TH: tyrosine hydroxylase; TRITC: tetramethylrhodamine isothiocyanate.

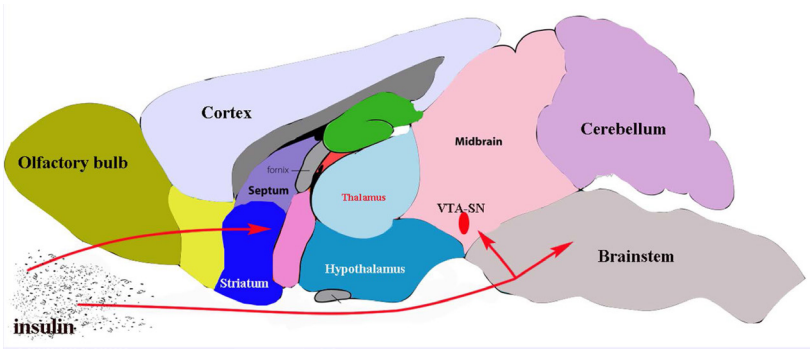

Figure 5 A schematic illustration of pathways for nose-to-brain insulin transport.
The olfactory and trigeminal nerves are two major routes (red arrows) that initially transport intranasal insulin into the brain parenchyma. Anatomically, the ventral tegmental area (VTA)-substantia nigra (SN) sits at the most ventral part of the midbrain and is in proximity with the brainstem, making it possible to retain a relatively high concentration of insulin diffused from the brainstem *via* interstitial fluid.

used exclusively in animal models and clinical trials to test therapeutics of insulin in CNS disorders. Although the effectiveness of intranasal brain delivery is known for decades, studies on the pharmacokinetics of macromolecules are limited. One of the early brain distribution studies showed that I^{125}-interferon-β1b (an 18.5 kDa peptide) was detected in the cerebral spinal fluid (CSF) of monkeys as early as 30 minutes upon intranasal administration (Thorne et al., 2008). Subsequently, Born et al. (2002) reported that upon nasal insulin spray (40 IU) in human subjects, there was a rapid accumulation of insulin in the CSF, which started to rise at 10 minutes, peaked at 30 minutes, and remained significantly elevated at 80 minutes. Because the accumulation of insulin in the CSF is likely delayed in relative to the parenchyma, these studies suggest that insulin might reach brain tissue rather rapidly (*e.g.*, within 30 minutes) through certain novel routes. Consistent with this notion, here we demonstrated a fast brain insulin transport in rats that peaked around 15–30 minutes following intranasal administration. Although insulin levels declined substantially from 15 minutes afterward, it remained significantly higher than baseline levels at 6 hours in several brain regions.

The olfactory and trigeminal nerves, both innervate the nasal cavities, are known to be responsible for the nose to brain drug transports. At the cellular level, it is proposed that either intracellular (*via* axons of olfactory and trigeminal nerves) or extracellular (*via* interstitial fluid) mechanisms are involved. The rapid rate of transport, as observed in human (Born et al., 2002), monkeys (Thorne et al., 2008), as well as rats in our study, strongly favor the extracellular mechanism, since the speed of retrograde axonal transport is rather slow (Maday et al., 2014). It is likely that other mechanisms are also involved in promoting high speed extracellular transport, as simple diffusion through extracellular space is still a slow process. For example, Iliff et al. (2013) proposed that such fast movement of macromolecules through interstitial fluid might be driven by a pump mechanism such as the pulse of blood flow.

An interesting observation in this study is that Alex546-insulin exclusively binds to neurons but not glial cells. An early study reported that in rats, the vast majority IR immunoreactivity co-localized with neurons, including CA1/CA2 pyramidal neurons in the hippocampus and somatostatin$^+$ neurons in the hypothalamus, but not GFAP$^+$ astrocytes (Unger et al., 1989). Neurons and synaptic membranes mainly express IR-A isoform, but the expression of IR on glial cells is less defined. Regard IR distribution, ^{125}I-insulin binding sites were found in the OB, neocortex, basal ganglia, hypothalamus, and the cerebellum of rat brain (Hill et al., 1986). Similarly, abundant IR mRNA signals were observed in the OB, cerebellum, dentate gyrus, hippocampus, piriform cortex, choroid plexus, and hypothalamus (Marks et al., 1990). In our study, brain regions with Alex546-Ins binding are mostly consistent with IR distributions reported in the above papers, except the cerebral cortex. Although Alex546-binding cells were noted in deep layers (V to VI) of the cerebral cortex, the outer layers (I to IV) were almost devoid of florescence signals. There was, however, a minimal amount of insulin detected in the cerebral cortex at 1 hour by ELISA, although it was not statistically different from baseline levels, possibly due to two factors. First, a large volume of the whole cortex used in protein extraction might lead to a further dilution of insulin concentration, which was already much lower in the deep layer as compared to other regions. Second, because the variation of insulin contents between individual animal is rather large while the sample size is relatively small, the power may not be sufficient to detect statistically significant differences in the cortex. Although this is also true for other regions, their large effect sizes offset this limitation and allow detecting statistical significance when compared to the baseline control (which is zero). Nevertheless, based on our findings, we proposed a model by which intranasal insulin reaches brain parenchyma. As shown in **Figure 5**, rh-Ins first reaches the OBs and brainstem *via* extracellular transport mechanisms and then diffuses towards adjacent structures at a rather fast speed.

In addition to general brain distribution, we were particularly interested in determining the bioavailability of insulin in the SN following intranasal administration. We provide evidence that intranasal insulin could reach the SN-VTA region. Since SN is in close proximity to the brainstem, it is likely insulin diffused to the SN from the brainstem, which retained the highest insulin levels among all brain regions examined. This suggests that the trigeminal nerve is quite efficient in insulin transport, at least in rats. Moreover, we found that pAkt is activated in a subset of Alex546-Ins binding DA neurons in the SN further indicating that insulin is sufficient to initiate downstream biological responses in these DA neurons. Large bodies of studies demonstrated that insulin could protect cultured neurons against a variety of insults. For example, insulin protected cultured cortical neurons against serum deprivation-induced apoptosis by activating the PI3K/Akt but was independent of the MAPK pathway (Ryu et al., 1999). Similarly, insulin was protective of cultured retinal neurons against H_2O_2-induced apoptosis (Yu et al., 2006). In addition to neurotropic and/or anti-apoptotic effects, insulin also modulates the releasing of a number of neurotransmitters including dopamine, norepinephrine, and GABA *via* activating synaptic IR (Gralle, 2017). These effects may provide benefits in ameliorating symptoms such as depression and sleep dysregulation, which are common in major neurodegenerative disorders.

In summary, data from this study along with our previous work (Pang et al., 2016) provide strong evidence that intranasal insulin could effectively reach deep brain structures including the nigrostriatal pathways, where it binds to DA neurons and activate intracellular cell survival signaling to counteract DA neurodegeneration. Furthermore, the multiple central actions of insulin and practical intranasal application make it a potential treatment option for other neurodegenerative disorders beyond AD and PD.

Author contributions: *Study design: YP; experiment implementation: LWF, KC, and YP; data analysis and interpretation: AB and YP; manuscript writing: LWF, AB, and YP. All authors approved the final version*

of the manuscript.
Conflicts of interest: *None declared.*
Financial support: *This study was supported by Michael. J. Fox Foundation (to YP). The funder had no involvement in the study design; data collection, analysis, and interpretation; paper writing; or decision to submit the paper for publication.*
Institutional review board statement: *This study was approved by the Institutional Animal Care Committee at the University of Mississippi Medical Center (protocol 1333A) on June 29, 2015 and conducted in strict accordance with the National Institutes of Health Guide for the Care and Use of Laboratory Animals.*

Data sharing statement: *Datasets analyzed during the current study are available from the corresponding author on reasonable request.*
Plagiarism check: *Checked twice by iThenticate.*
Peer review: *Externally peer reviewed.*

Open peer reviewer: *Chih-Li Lin, Chung Shan Medical University, Institute of Medicine, Taiwan, China*
Additional file: *Open peer review report 1.*

References

Avgerinos KI, Kalaitzidis G, Malli A, Kalaitzoglou D, Myserlis PG, Lioutas VA (2018) Intranasal insulin in Alzheimer's dementia or mild cognitive impairment: a systematic review. J Neurol 265:1497-1510.

Barua N, Gill S (2018) Drug Delivery for Movement Disorders. Prog Neurol Surg 33:243-252.

Born J, Lange T, Kern W, McGregor GP, Bickel U, Fehm HL (2002) Sniffing neuropeptides: a transnasal approach to the human brain. Nat Neurosci 5:514-516.

Brabazon F, Wilson CM, Jaiswal S, Reed J, Frey WH Nd, Byrnes KR (2017) Intranasal insulin treatment of an experimental model of moderate traumatic brain injury. J Cereb Blood Flow Metab 37:3203-3218.

Domanskyi A, Saarma M, Airavaara M (2015) Prospects of neurotrophic factors for Parkinson's disease: comparison of protein and gene therapy. Hum Gene Ther 26:550-559.

Ghasemi R, Haeri A, Dargahi L, Mohamed Z, Ahmadiani A (2013) Insulin in the brain: sources, localization and functions. Mol Neurobiol 47:145-171.

Gralle M (2017) The neuronal insulin receptor in its environment. J Neurochem 140:359-367.

Hill JM, Lesniak MA, Pert CB, Roth J (1986) Autoradiographic localization of insulin receptors in rat brain: prominence in olfactory and limbic areas. Neuroscience 17:1127-1138.

Iliff JJ, Wang M, Zeppenfeld DM, Venkataraman A, Plog BA, Liao Y, Deane R, Nedergaard M (2013) Cerebral arterial pulsation drives paravascular CSF-interstitial fluid exchange in the murine brain. J Neurosci 33:18190-18199.

Lioutas VA, Alfaro-Martinez F, Bedoya F, Chung CC, Pimentel DA, Novak V (2015) Intranasal insulin and insulin-like growth factor 1 as neuroprotectants in acute ischemic stroke. Transl Stroke Res 6:264-275.

Maday S, Twelvetrees AE, Moughamian AJ, Holzbaur EL (2014) Axonal transport: cargo-specific mechanisms of motility and regulation. Neuron 84:292-309.

Mamik MK, Asahchop EL, Chan WF, Zhu Y, Branton WG, McKenzie BA, Cohen EA, Power C (2016) Insulin treatment prevents neuroinflammation and neuronal injury with restored neurobehavioral function in models of HIV/AIDS neurodegeneration. J Neurosci 36:10683-10695.

Marks JL, Porte D Jr, Stahl WL, Baskin DG (1990) Localization of insulin receptor mRNA in rat brain by in situ hybridization. Endocrinology 127:3234-3236.

Pang Y, Lin S, Wright C, Shen J, Carter K, Bhatt A, Fan LW (2016) Intranasal insulin protects against substantia nigra dopaminergic neuronal loss and alleviates motor deficits induced by 6-OHDA in rats. Neuroscience 318:157-165.

Patel MM, Patel BM (2017) Crossing the blood-brain barrier: recent advances in drug delivery to the brain. CNS Drugs 31:109-133.

Pomytkin I, Costa-Nunes JP, Kasatkin V, Veniaminova E, Demchenko A, Lyundup A, Lesch KP, Ponomarev ED, Strekalova T (2018) Insulin receptor in the brain: Mechanisms of activation and the role in the CNS pathology and treatment. CNS Neurosci Ther 24:763-774.

Purves D, Augustine GJ, Fitzpatrick D, Katz LC, LaMantia A, McNamara J, Williams MS (2001) Neuroscience. 2nd ed. Sunderland (MA): Sinauer Associates.

Ramalingam M, Kim SJ (2016) The neuroprotective role of insulin against MPP(+)-induced Parkinson's disease in differentiated SH-SY5Y cells. J Cell Biochem 117:917-926.

Ryu BR, Ko HW, Jou I, Noh JS, Gwag BJ (1999) Phosphatidylinositol 3-kinase-mediated regulation of neuronal apoptosis and necrosis by insulin and IGF-I. J Neurobiol 39:536-546.

Sampaio TB, Savall AS, Gutierrez MEZ, Pinton S (2017) Neurotrophic factors in Alzheimer's and Parkinson's diseases: implications for pathogenesis and therapy. Neural Regen Res 12:549-557.

Shah L, Yadav S, Amiji M (2013) Nanotechnology for CNS delivery of bio-therapeutic agents. Drug Deliv Transl Res 3:336-351.

Smith PK, Krohn RI, Hermanson GT, Mallia AK, Gartner FH, Provenzano MD, Fujimoto EK, Goeke NM, Olson BJ, Klenk DC (1985) Measurement of protein using bicinchoninic acid. Anal Biochem 150:76-85.

Sulivan AM, O'keeffe GW (2016) Neurotrophic factor therapy for Parkinson's disease: past, present and future. Neural Regen Res 11:205-207.

Thorne RG, Hanson LR, Ross TM, Tung D, Frey WH 2nd (2008) Delivery of interferon-beta to the monkey nervous system following intranasal administration. Neuroscience 152:785-797.

Unger J, McNeill TH, Moxley RT 3rd ,White M, Moss A, Livingston JN (1989) Distribution of insulin receptor-like immunoreactivity in the rat forebrain. Neuroscience 31:143-157.

Yu XR, Jia GR, Gao GD, Wang SH, Han Y, Cao W (2006) Neuroprotection of insulin against oxidative stress-induced apoptosis in cultured retinal neurons: involvement of phosphoinositide 3-kinase/Akt signal pathway. Acta Biochim Biophys Sin (Shanghai) 38:241-248.

Zemva J, Schubert M (2014) The role of neuronal insulin/insulin-like growth factor-1 signaling for the pathogenesis of Alzheimer's disease: possible therapeutic implications. CNS Neurol Disord Drug Targets 13:322-337.

Zhou Y, Peng Z, Seven ES, Leblanc RM (2018) Crossing the blood-brain barrier with nanoparticles. J Control Release 270:290-303

P-Reviewer: Lin CL; C-Editors: Zhao M, Li CH; T-Editor: Liu XL